Orientational Switch of The Lipase A Enzyme at The Oil-water Interface: An Order of Magnitude Increase in Turnover Rate with a Single Surfactant Tag Explained

Sudip Das, Sudarshan Behera, and Sundaram Balasubramanian*

Chemistry and Physics of Materials Unit

Jawaharlal Nehru Centre for Advanced Scientific Research, Bangalore 560 064, India

E-mail: bala@jncasr.ac.in

*To whom correspondence should be addressed

Contents

1 Summary of experimental observations reported by Kubler et al[1]

Table S1: Turnover rate (in $\mu M^{-1}s^{-1}$ unit) of LipA for the hydrolysis of 4-MU oleate substrate in water in presence of Thesit detergent, calculated from a kinetic model for interfacial catalysis developed from experiments by Kubler et al.[1] The first subscript of TO refers to enzyme and the second subscript refers to substrate (f: free substrate or free enzyme; mon: enzyme bound to monomeric detergent; mic: enzyme bound to micelle; b: substrate bound to micelles).

pH	$\mathbf{TO}_{f,f}$	$\mathbf{TO}_{mon,f}$	$\mathrm{TO}_{mic,f}$	$\mathrm{TO}_{f,b}$	$\mathbf{TO}_{mon,b}$	$\mathrm{TO}_{mic,b}$
8.5	**1.9 ± 0.2**	0.4 ± 0.4	0.0 ± 0.0	0.0 ± 0.0	**27.0 ± 9.0**	0.0 ± 0.0
10.0	**1.7 ± 0.5**	**21.7 ± 1.1**	0.0 ± 0.0	0.7 ± 9.9	0.0 ± 0.0	0.0 ± 0.0

2 Immobilization of enzymes

Various immobilization strategies of enzymes and their efficacies as reported in literature is summarized below.

Enzyme	**Immobi -lization method**	**Immobi -lizing material**	**Catalytic reaction type**	**Activity increase (in folds)**	**Reference**
LipA 8M (octapole mutant)	covalent binding	Fe_3O_4 nano-particles	hydrolysis	0.34-1.68	[2]
LipA	genetic fusion	modified Cry3Aa crystal	trans-esterification	2.21	[3]
Recombinant *Bacillus subtilis*	covalent binding	magnetic nano-particles	hydrolysis	0.64	[4]

lipase					
lipases from *C. antarctica* (lipase B), *C. cylindracea*, *P. cepacia*, *P. fluorescens* and hog pancreas	adsorption, cross -linking	chitosan or ultrasound -treated chitosan or chitosan activated with glutaraldehyde	hydrolysis	0.64-0.83	[5]
Porcine pancreatic lipase	adsorption (through covalent bond)	chitosan	alcoholysis	0.31-0.40	[6]
Porcine pancreatic lipase	adsorption (through covalent bond), cross -linking	chitin chitosan	hydrolysis	0.14 0.15	[7]
Porcine pancreatic lipase	adsorption (through covalent bond), cross -linking	chitin chitosan	esterification	4.25 2.06	[7]
lipoprotein lipase	adsorption covalent	PEG PEG	Acetylation	1.00 **58.33**	[8]

	-binding				
	carrier-fixed enzyme	-		**38.33**	
Pseudomonas cepacia lipase	carrier-fixed enzyme	-	Acetylation	0.53	
Candida antarctica lipase B	carrier-fixed enzyme	-	Acetylation	2.35	
Porcine pancreatic lipase	covalent binding	polysiloxane and polyvinyl alcohol hybrid matrix	synthesis of surfactants and biodiesel	**9.21**	[9]
Candida rugosa lipase	repeated absorption	bacterial cellulose membrane	hydrolysis	0.94	[10]
Candida antarctica lipase A	adsorption, cross -linking	octyl-agarose and poly-ethyleneimine	hydrolysis	**7.00**	[11]
Eversa lipase	adsorption cross -linking	octyl-agarose and poly-ethyleneimine	hydrolysis	1.50	[12]
Mucor miehei lipase	**adsorption**	Octadecyl -Sepabeads	hydrolysis	**20.00**	[13]
Rhizomucor	covalent	reduced	hydrolysis	2.00	[14]

miehei lipase	binding (coimmobili -zation with *Pseudomonas fluorescens* lipase	glyoxyl-octyl-PFL			
Thermomyces lanuginosus lipase	adsorption, amination and intra-molecular cross-linking of lipase surface	Aldehyde -Dextran	hydrolysis	6.47	[15]
Cellulose binding domain protein and *Geobacillus stearo-thermophilus lip* gene	bio -affinity based binding	cellulosic nanogel	hydrolysis	1.24	[16]
Pseudomonas cepacia lipase	precipitation-cross-linking	magnetic cellulose nanocrystals	hydrolysis	1.33-1.60	[17]
Porcine pancreas lipase	adsorption	Surface -modified nano-sized	hydrolysis	0.93-1.55	[18]

		magnetite particles			
Candida rugosa lipase	ionic adsorption	Magnetic silica nanoparticles supported ionic liquids	esterification	1.18	[19]
Burkholderia cepacia lipase	micro-capsulation	poly-ethyleneimine microcapsules modified with oxidized multiwall carbon nanotubes	esterification	**21.90**	[20]
LipA	covalent binding	poly-(sulfobetaine methacrylate) brushes	hydrolysis	**100.00**	[21]

Table S2: A short survey of the recent literature on the immobilization of enzymes. Significant enhancements in activity through immobilization are shown in bold face.

3 Solvent accessible surface area (SASA)

Table S3: Total and hydrophobic solvent accessible surface area (SASA) of LipA and of its head cap and major side regions in bulk water and at the oil-water interface (at both 0DET and 1DET conditions) at pH 8.5 and 10. 0DET: No detergent; 1DET: Contains one detergent molecule.

pH	System or Region	Type	SASA (Å^2)		
			Bulk	Interface (0DET)	Interface (1DET)
8.5	Enzyme	Total	8470 (100 %)	8556 (100 %)	8665 (100 %)
		Hydrophobic	3433 (41 %)	3535 (41 %)	3569 (41 %)
	Head cap	Total	3863 (46 %)	3929 (46 %)	3981 (46 %)
		Hydrophobic	1885 (22 %)	1980 (23 %)	1995 (23 %)
10	Enzyme	Total	8431 (100 %)	8426 (100 %)	8623 (100 %)
		Hydrophobic	3394 (40 %)	3453 (41 %)	3546 (41 %)
	Head cap	Total	3864 (46 %)	3875 (46 %)	4051 (47 %)
		Hydrophobic	1873 (22 %)	1946 (23 %)	2009 (23 %)

4 Definition and calculation of some terms

4.1 Head cap region of LipA

Residues constituting the head cap region were identified based on the all-atom MD simulation trajectories of LipA in bulk water with thirty detergent molecules at pH8.5 reported earlier.[22] In those AA MD simulations of one LipA enzyme soaked in bulk water along with thirty Thesit molecules, the latter were found to aggregate. At pH 8.5, this aggregate was seen to predominantly interact with the head cap residues and at pH 10 with the residues of the side region of LipA. At pH 8.5, residues whose Cα atom had more than 20 % probability of being found within a 2 Å distance from any atom of any of the thirty detergent molecules are considered to constitute the head cap region. The same geometric criterion was applied to find out the residues constituting the major side region, but from the trajectory at pH 10. The primary sequence index of the residues in the respective regions of LipA are provided in Table S4.

Table S4: Residues constituting the head cap and major side regions of LipA.[22] At pH 8.5, the side chain of residues Lys23 (charge: +1) and Tyr139 (charge: 0) are protonated, whereas they are deprotonated at pH 10 (charge: 0 and -1, respectively).

Region of LipA	Residue index	Total charge at pH 8.5	Total charge at pH 10
Total	1-181	+3.0	+1.0
Head cap	10-20, 40-55, 75-90, 102-110, 130-140, 150-165	+0.0	-1.0
Major side	13-67	+1.0	0.0

4.2 Interfacial energy of LipA, E_I

The contribution of LipA to the interfacial energy is E_I = -γS, where γ is the octane-water interfacial tension[23] and S is the area occupied by the enzyme's coarse-grained beads within the interface (beads whose center of mass are located wihtin the interface width). The diameter of these beads and the interface width were both taken from the van der Waals diameter (4.7 Å) of the coarse-grained polarizable bead[24,25]). The location of the interface was defined as the position along the z direction at which the density of water equals the density of oil.

4.3 Change in protein-solvent interaction energy, ΔE_{PS}

ΔE_{PS} was defined as the sum of the water-to-oil transfer free energies of the amino acid sidechains exposed to oil. The sum includes those residues whose sidechain are located within the oil region (calculated as the number of residues whose side-chain centers of mass are within 5 Å from any bead of octane), and it excludes the buried ones,[26] defined as those having a solvent accessible surface area lower than 30 Å^2 with respect to the oil phase. The values of the water-to-oil transfer free energies of the individual amino acid sidechains were obtained from the literature.[27,28]

4.4 Change in intra-protein interaction energy, ΔE_{PP}

The change in protein-protein self-interaction energy upon adsorption to the interface was calculated by substracting the intra-protein interaction energy in bulk water from the same at the interface.

4.5 Number of contacts of LipA with oil phase, N_c

The interaction of the enzyme with the oil phase was calculated as the number of contacts wihtin a cut-off distance 5 Å of the enzyme beads with the oil beads including the aliphatic tail of the detergent.

4.6 Hydrophobic moment, μ

The hydrophobic dipole moment is a vector with dimensions of energy and measures the anisotropic arrangements of side-chains within the secondary structure element of a protein.[29] A large magnitude of the modulus of this moment indicates a highly anisotropic arrangement of residues within the structure. The direction of this dipole corresponds to the average direction of the hydrophobic residues. The hydrophobic moment μ is defined as[29] $\sum_i H_i \hat{s}_i$ where the sum runs over the residues in the head cap region, H_i is a measure of the hydrophobicity of residue i (in the present study, the oil-water partitioning free energy[27,28]), while $\hat{s}_i$ is the unit vector pointing from the residue alpha carbon to the center of mass of its sidechain.

All these terms (E_I, ΔE_{PS}, ΔE_{PP}, N_c and μ) reported here were calculated by averaging over equilibrium MD trajectories of all the ten independent configurations for each systems. These trajectories with LipA adsorbed at the interface were long enough (2000 to 5000 ns) compared to the autocorrelation time for the enzyme reorientation (100 ns, Figure 3b in the main text).

5 Supplementary Figures and Tables

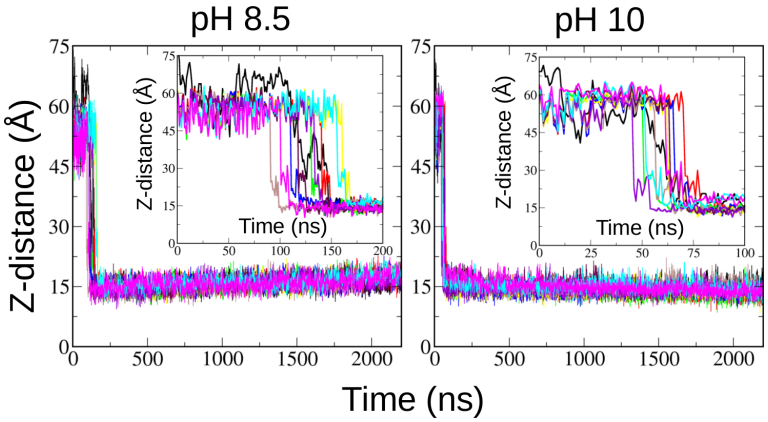

Figure S1: Time evolution of the z-distance of LipA in ten independent normal MD simulation trajectories at pH 8.5 and 10. At t=0, the enzyme is in bulk water. The time when LipA gets adsorbed to the interface is zoomed in the inset.

Table S5: The component of the hydrophobic moment of the head cap region of the enzyme along interface normal, μ_z (in kcal/mol) and corresponding free energy of adsorption at the interface (in brackets) (in kcal/mol). For the definition of hydrophobic moment μ_z, see Section 4.6 of SI.

System or pH	pH 8.5	pH 10
0DET_bulk	3.44 (0.00)	0.25 (0.00)
0DET_intf	30.94 (-8.00)	17.24 (-6.00)
1DET_intf	41.71 (-16.00)	24.36 (-16.00)

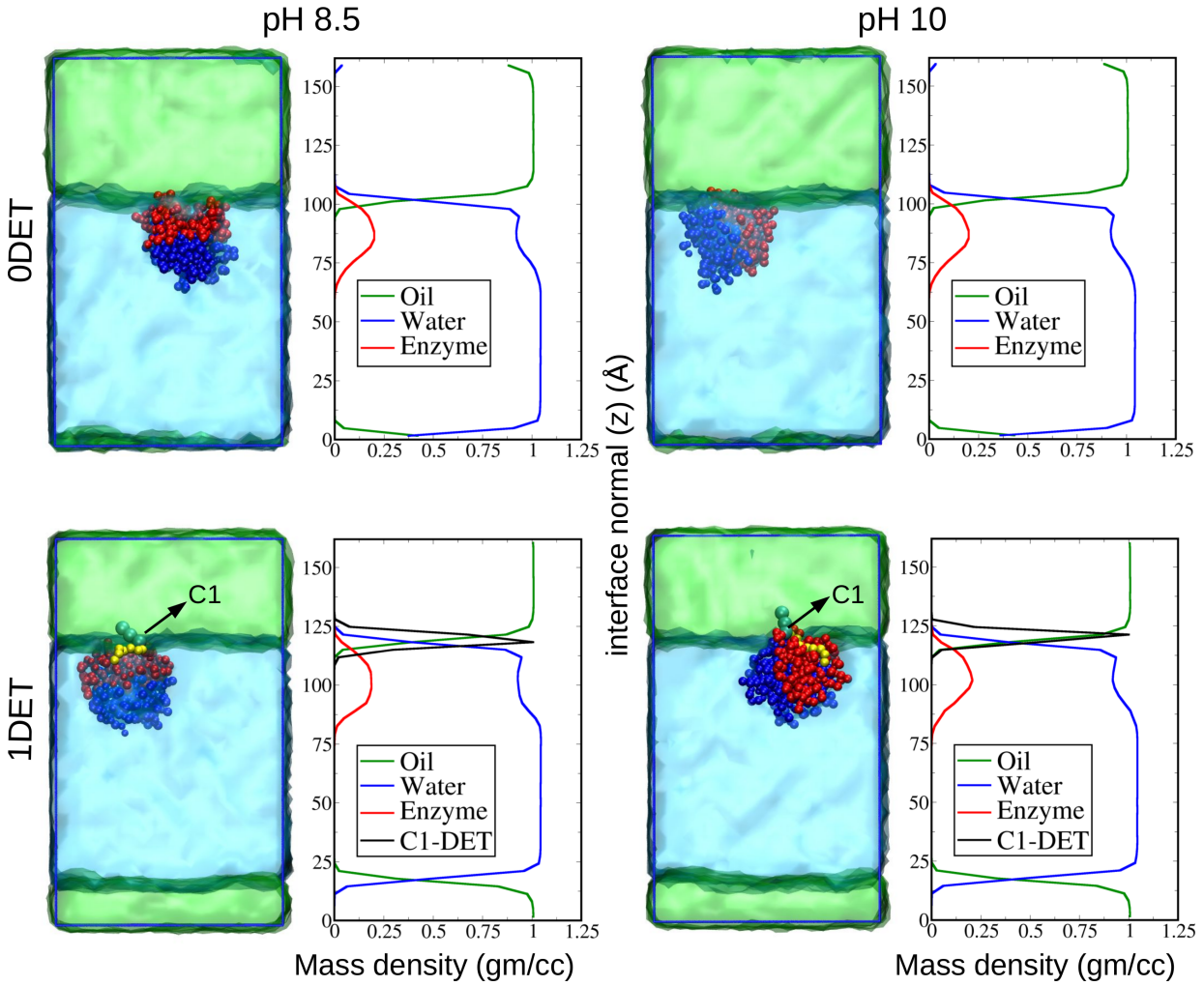

Figure S2: Simulation snapshots and density profiles across the interface normal for different component of the systems both in the absence and presence of a detergent molecule at both pH 8.5 and 10. The aliphatic chain and PEG part of the detergent are shown as green and yellow beads, respectively. Rest of the color scheme follows Figure 1 in the main text. The mass density of bulk water obtained from our simulations (1.04 gm/cc) matches well with the mass density reported for the polarizable MARTINI model for water.[25] The mass density of the C1 bead of detergent molecule is plotted after multiplying it by a factor of 10^3.

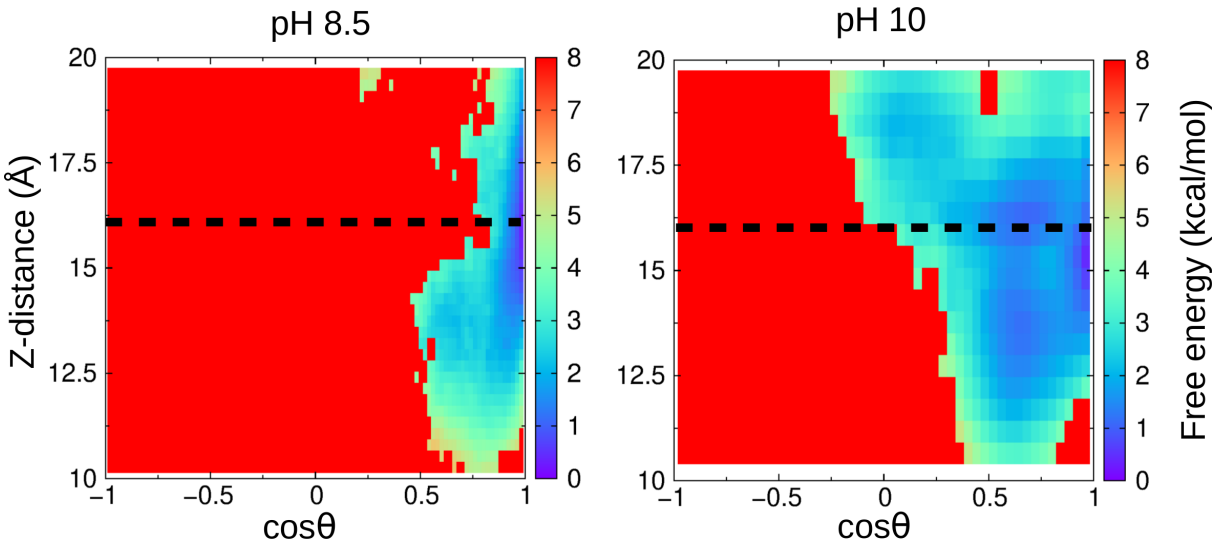

Figure S3: Two dimensional free energy profile of LipA near the interface as a function of z-distance and cosine of the orientational angle θ calculated from umbrella sampling simulations at pH 8.5 and 10, by placing the umbrellas only along the z-distance. These plots represent the switchability of LipA via pH. The black dotted line represents the state where LipA gets adsorbed to the interface. The data is same as in Figure 2b of the main text, but is zoomed in near the interface region.

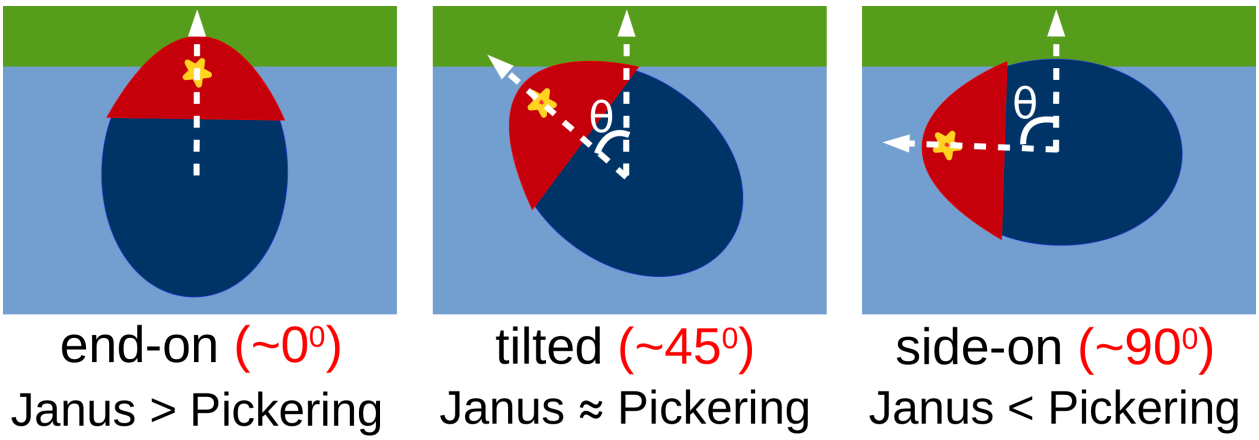

Figure S4: Posssible orientations of LipA at the oil-water interface.

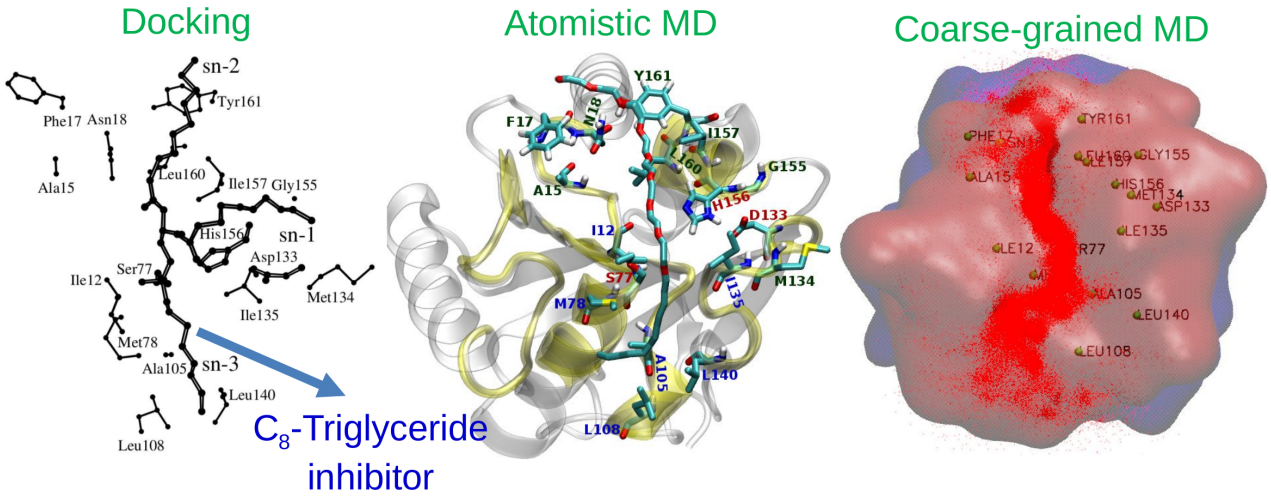

Figure S5: Left: Docking of C_8-triglyceride inhibitor onto the active site of LipA[30] (reprinted with permission from Elsevier). Middle: Residues binding the monomeric Thesit detergent at the active site of LipA obtained from atomistic MD simulation in bulk water at pH 8.5[22] (reprinted with permission from American Chemical Society). Right: Scatter plot of PEG beads (red points) of monomeric detergent over the head cap (red surface) of LipA (blue surface) present at the oil-water interface at pH 8.5 observed from the current CGMD simulations. The backbone bead of residues interacting with the detergent are shown in green spheres. This scatter plot is constructed after combining trajectories from ten independent MD runs at coarse-grained level in a body-fixed representation of the lipase. The orientation of LipA in all figures are the same . These figures together show that the monomeric detergent binds to the substrate-binding pocket of LipA at pH 8.5.

6 Supplementary discussion

6.1 Quantification of the Janus character

The distributions of E_I and of ΔE_{PS} shown in Figure S6 are asymmetric and can be resolved into a sum of two normal distributions. Based on their respective mean values, these distributions can be identified as arising out of *end-on* and *tilted* orientations of LipA at the interface. E_I is more stable at the tilted than at the end-on orientation (Table S6). At pH 8.5, the stabilization gained from ΔE_{PS} in the end-on orientation is larger than the destabilization at tilted orientation (Figure S6b and Table S6). This is due to the heterogeneous surface polarity (Table S3) as well as an overall neutral head cap region and charged side region (Table S4). Similarly, the distribution of E_I favors an end-on orientation (Figure S6a). Thus, together, E_I and ΔE_{PS} make the end-on orientation most likely at pH 8.5 (Figure 3a). At pH 10, an overall neutral side region and a charged head cap region (Table S4) makes ΔE_{PS} to be stabilizing and more probable in the tilted orientation; E_I too favors the same. Thus, the tilted orientation is most probable at pH 10 (Figure 3a).

6.2 Adsorption free energy

To understand the reasons behind the identical adsorption free energy of LipA towards the interface in the presence of monomeric detergent at different pH values, different energies contributing to the adsorption free energy, i. e., E_I, ΔE_{PS} and ΔE_{PP} have to be looked into (Table S6). Except for ΔE_{PP}, the extent of change in other energies upon change in pH are more or less comparable between the systems in the absence and in the presence of monomeric detergent (Table S6). However, in the absence of the detergent, there is a significant change in the value of ΔE_{PP} at pH 10 (21.0 kcal/mol) with respect to the same at pH 8.5 (10.5 kcal/mol) (Table S6). At pH 10, LipA, remaining mostly in the tilted orientation (Figure 3a), interacts with the interface mainly through the side region which is populated more with hydrophilic residues. This orientation thus requires the exposure of

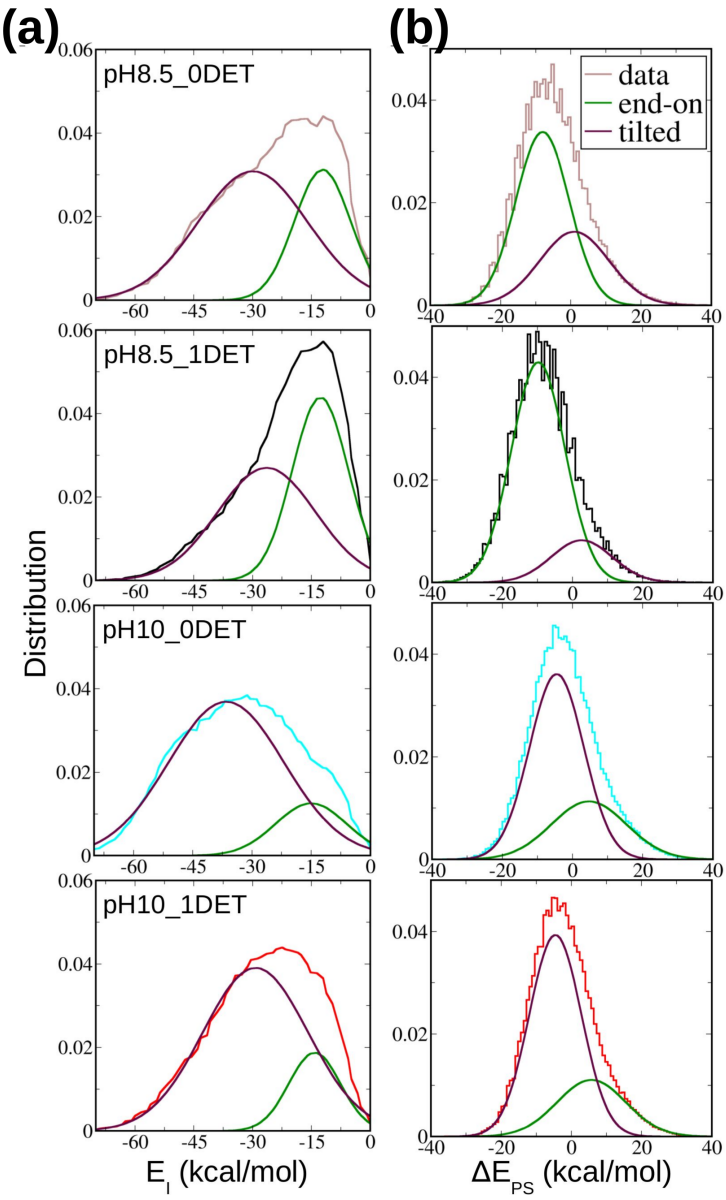

Figure S6: Overall and orientation-specific distribution of (a) the interfacial energy of the enzyme, E_I and (b) the change in protein-solvent interaction energies upon adsorption of the enzyme to the interface, ΔE_{PS} (b). The orientation-specific distributions were obtained by fitting the overall distribution to a sum of two Gaussians. The overall distributions follow the same color scheme as used in Figure 3b; i. e., pH8.5_0DET: pale brown, pH8.5_1DET: black, pH10_0DET: cyan and pH10_1DET: red. The end-on and tilted orientations are represented as green and maroon, respectively for all the systems. For the definition of E_I and ΔE_{PS}, see Sections 4.2 and 4.3 of SI.

hydrophilic residues from the side region to the interface which results in the loss of stable intra-protein electrostatic contacts. This makes ΔE_{PP} highly destabilizing (21 kcal/mol) at pH 10 in the absence of detergent. However, in the presence of monomeric detergent, the stable intra-protein electrostatic contacts are restored due to the polar environment around the side region induced by the polar, PEG part of the detergent. This results in ΔE_{PP} to be comparable between the systems at pH 8.5 (5.3 kcal/mol) and pH 10 (8.6 kcal/mol), in the presence of monomeric detergent (Table S6). The presence of the detergent makes these energies at both pH values closer to each other, yielding identical adsorption free energies.

The increase in total SASA of LipA upon adsorption at the interface (Table S3) is attained through the loss of some stabilizing intra-protein contacts. As a result, the change in intra-protein interaction energy upon adsorption at the interface from bulk water (ΔE_{PP}) is positive (Table S6). The sum of E_I, ΔE_{PS} and ΔE_{PP} follows the same trend as the free energy of adsorption of LipA to the interface from bulk water (ΔG_{ads}) (Table S6), suggesting an enthalpic basis for interfacial affinity.

Table S6: Most probable values of different energies (in kcal/mol) and contacts controlling the reorientational switch of the enzyme at oil-water interface. E_I: interfacial energy of the enzyme, ΔE_{PS} and ΔE_{PP}: change in protein-solvent and intra-protein interaction energy (respectively) upon adsorption of the enzyme to the interface, total: $E_I+\Delta E_{PS}+\Delta E_{PP}$, N_c: number of contacts: counts the number of contacts between enzyme and the oil phase including the aliphatic tail of the detergent. For the definition of E_I, ΔE_{PS}, ΔE_{PP} and N_c, see Sections 4.2, 4.3, 4.4 and 4.5 of SI.

System or proper-ty	pH8.5						pH10					
	0DET			1DET			0DET			1DET		
	end-on	tilt-ed	avg.	end-on	tilt-ed	avg.	end-on	tilt-ed	avg.	end-on	tilt-ed	avg.
E_I	-12.2	-29.9	-18.2	-12.7	-26.4	-15.4	-13.9	-36.5	-30.8	-14.2	-29.3	-25.5
ΔE_{PS}	-8.1	1.0	-5.4	-9.7	2.6	-8.8	4.7	-4.5	-2.4	5.7	-4.6	-3.5
ΔE_{PP}	-	-	10.5	-	-	5.3	-	-	21.0	-	-	8.6
total	-	-	-13.1	-	-	-18.9	-	-	-12.2	-	-	-20.4
ΔG_{ads}	-	-	-8.0	-	-	-16.0	-	-	-6.0	-	-	-16.0
N_c	-	-	17.7	-	-	19.3	-	-	26.7	-	-	29.2

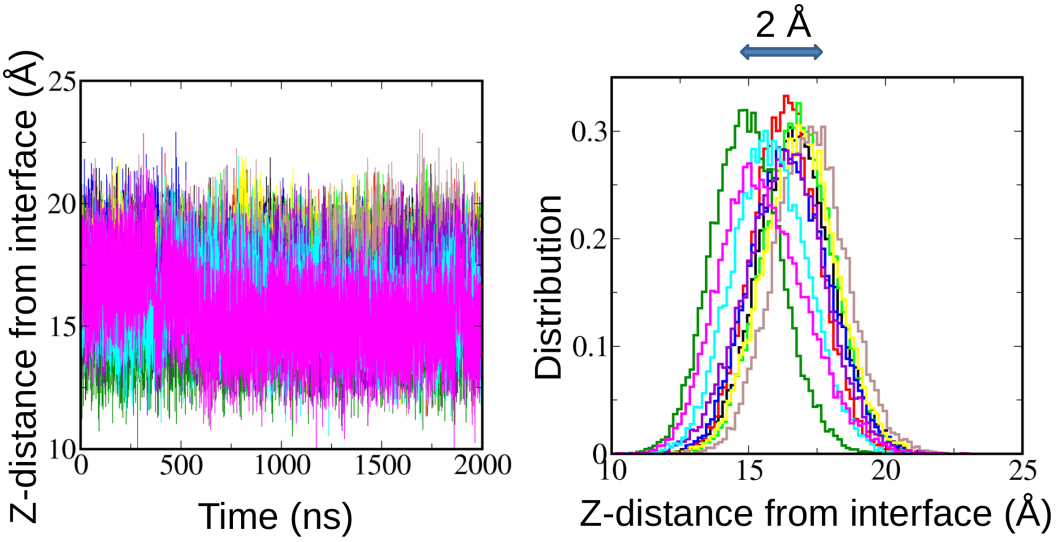

Figure S7: Time evolution and the distribution of z-distance of the center of mass of LipA from the interface at pH 8.5 after it gets bound to the interface.

7 Computational details

7.1 System preparation

The X-ray crystal structure of substrate-free LipA (PDB ID: 1i6w[30]), was taken from RCSB protein data bank.[31] Although LipA exists as a homodimer in 1i6w, it is not a functional dimer and exists mostly as a monomer in the solution.[30] So, only chain A (the most abundant conformation in solution[30]) from this homodimeric protein was chosen for the present study. Two residues (Ala1 and Glu2) were missing in this structure (chain A). The coordinates for atoms in Glu2 were taken from another representative structure (chain B), whereas the same for Ala1 were generated by PyMOL.[32] The protonation state of each residue in the protein at pH 8.5 and 10 was determined using the ProteinPrepare tool available in PlayMolecule repository.[33] At pH 8.5, the side chain of residues Lys23 (charge: +1) and Tyr139 (charge: 0) are protonated, whereas, they are deprotonated at pH 10 (charges 0 and -1 respectively). The crystal structure of Thesit detergent (C12E8) was obtained from RCSB ligand explorer.

The initial structures for the systems with one molecule of LipA both in bulk water (in absence of detergent) and in the oil-water biphasic system (separately with 0, 1, 5, and 20

numbers of detergent molecules) were created using PACKMOL software[34] at both pH 8.5 and 10. Ten independent initial configurations with different positions and orientations of the protein (and detergent) molecule(s) were prepared for each of these systems. Ions were added to neutralize the systems. Details of all the systems and compositions are summarized in Table S7.

Table S7: Details of all the LipA systems simulated. Each system contains one LipA molecule. Overall 460 microseconds of MARTINI CG-level simulations were carried out for the present study. Values in the parentheses for umbrella sampling and steered CGMD corresponds to the number of windows and independent pulling trajectories, respectively.

Run type	System type	pH	No. of detergent molecules	No. of solvent molecules (oil:water)	No. of independent runs	Run length (μs)	Mean box dimension (Å^3)
normal CGMD	in bulk water	8.5	0	0:8784	10	2.2	100.4x100.4x100.4
		10	0	0:8784	10	2.2	100.4x100.4x100.4
normal CGMD	oil-water bi-phasic	8.5	0	2224:7496	10	2.2	94.3x94.3x161.4
		10	0	2224:7496	10	2.2	94.4x94.4x161.1
		8.5	1	2224:7496	10	5.0	94.5x94.5x161.0
		10	1	2224:7496	10	5.0	94.4x94.4x161.2
		8.5	5	2224:7496	10	5.0	94.4x94.4x161.6
		10	5	2224:7496	10	5.0	94.4x94.4x161.5
		8.5	20	2224:7496	10	5.0	95.0x95.0x161.8
		10	20	2224:7496	10	5.0	95.0x95.0x161.6
umbrella sampling	oil-water bi-phasic	8.5	0	2224:7496	1 (20)	4.0	94.3x94.3x161.4
		10	0	2224:7496	1 (20)	4.0	94.4x94.4x161.1
		8.5	1	2224:7496	5 (20)	4.0	94.5x94.5x161.0
		10	1	2224:7496	5 (20)	4.0	94.4x94.4x161.2
steered CGMD	oil-water bi-phasic	8.5	0	2224:7496	1 (60)	12.0	94.3x94.3x161.4
		10	0	2224:7496	1 (60)	12.0	94.4x94.4x161.1

7.2 Force field

An elastic network model (ELNEDYN[35]) combined with MARTINI coarse-grained (CG) force field[36] was employed to obtain a realistic flexibility of the enzyme. MARTINI force

field developed for nonionic surfactants[37,38] was used for Thesit. As prescribed by this force field, the self-interaction between the 'SNa' beads was made more attractive to enhance the self-interaction between the polyethyleneglycol (PEG) part of detergent to the level of an 'Nda' bead.[37–39] As the 'SNa' type beads are present only in the EG groups of detergent, the self-interaction of other molecules present in the system would not be affected. A two-bead CG model extracted from the MARTINI solvent model was used for octane (oil). For water, we used a refined polarizable Martini model.[24,25] This model is applicable for oil-water biphasic system as well.[24] The MARTINI force field is well suited for the study of proteins at interfaces[40] as the amino acid parameters in this force field have been developed based on their experimental water-to-oil partitioning free energies;[36] the oil-water surface tension is also in good agreement with experiments.[41] The martinize.py script[36] was used to obtain the CG topology for the enzyme from its crystal structure.

7.3 Simulation protocol

7.3.1 Normal molecular dynamics (MD)

All the simulations were performed in the NAP_zT ensemble with a constant area of the interface almost perpendicular to the z-axis with 1 bar pressure only along the z-direction at a temperature of 300 K. The integration time step was increased from 2 to 20 fs in five steps of equilibrium simulation with a total runtime of 100 ns with a gradual decrease in the force constant for the position restraint on all heavy atoms of protein from 10^3 kcal/mol/rad^2 to zero. Bussi thermostat[42] and Berendsen barostat[43] was used for all these steps. Later, the equilibrated system went through a long production run (2.2 and 5.0 microseconds in absence and presence of detergent molecule(s), respectively) coupled with Bussi thermostat[42] and Parrinello-Rahman barostat[44,45] at 300 K temperature and 1 bar pressure, respectively. An integration time step of 20 fs was used. Three dimensional periodic boundary conditions were applied. As precribed by the refined polarizable force field[24] for water, particle mesh Ewald (PME) method[46] with cutoff distance of 11 Å was used to treat the long-range electrostatic

interactions in a medium of relative dielectric constant of 2.5. All systems were simulated using GROMACS 5.1.4.[47–52] All the data presented here were obtained from the analysis of the last two microseconds in each of the ten independent trajectories for each system.

7.3.2 Umbrella sampling

Umbrella sampling[53] simulations were performed for the system both with and without monomeric detergent molecule at both pH 8.5 and 10 to obtain the free energy of adsorption of LipA to the oil-water interface. In order to generate the initial configuration for the umbrellas, the center of mass of the enzyme was pulled towards the water phase relative to that of the oil phase at a speed of 0.1 Å/ns with a spring constant of 10^4 kJ/mol/nm^2. Twenty umbrella windows were made by extracting frames from the pulling simulation at different distances of the enzyme center of mass from the interface in such a way that these distances range from the interface to the bulk water. All these windows were run for 200 ns each by restraining the distance of the enzyme from the interface using a harmonic potential with a spring constant of 10^3 kJ/mol/nm^2. By this umbrella sampling technique, we aimed to sample different orientations of the enzyme from the interface to bulk water. The two-dimensional free energy surface along both the z-distance from the interface and the orientational angle θ was reconstructed by reweighting each observed configurations from all these umbrella windows using the weighted histogram analysis method (WHAM) implemented within the gmx_wham[54] code.

7.3.3 Steered MD

To validate the free energy profile obtained from umbrella sampling for the systems in the absence of detergent molecules, we performed steered MD simulations. The free energy profile for this steered MD simulations was reconstructed from a set of nonequilibrium force-probe simulations using the Jarzynski equality,[55] as implemented by Park and Schulten.[56] The center of mass of the enzyme was pulled towards the water phase relative to the center of

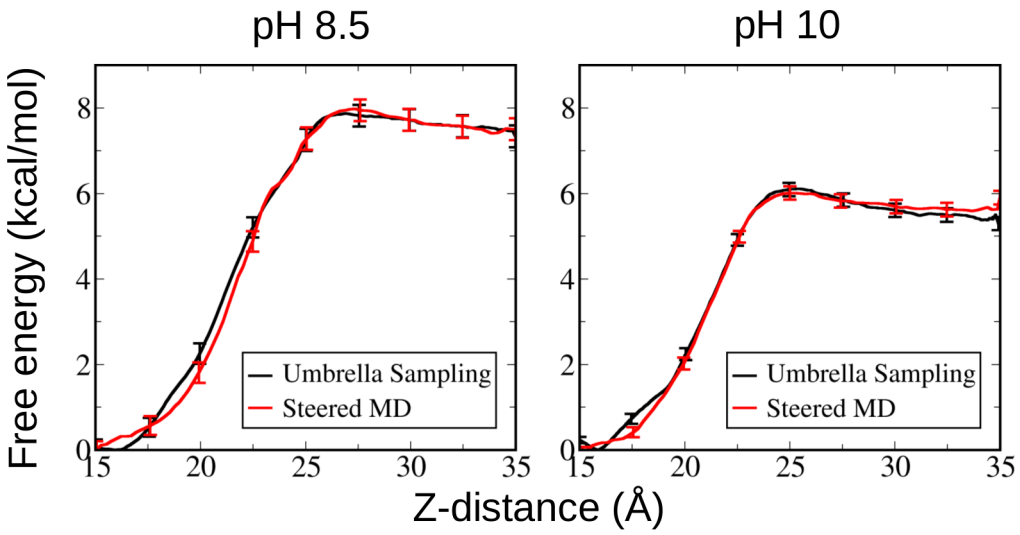

Figure S8: Free energy profile for the adsorption of LipA at the oil-water interface calculated separately from umbrella sampling and steered MD simulations at pH 8.5 and 10 in the absence of detergent.

mass of the oil phase at a speed of 0.1 Å/ns with a spring constant of 10^4 kJ/mol/nm^2. The choice of these values for the pulling speed and the spring constant satisfy the stiff-spring approximation and the cumulant expansion of the free energy found to be consistent with the result obatined from the Jarzynski equality.[56] This outcome ensures a sufficient sampling of the pulling simulations (60 independent pulling trajectories for each system) to estimate a reliable free energy profile.[56] Figure S8 shows that both umbrella sampling and steered MD yield the same free energy profiles.

7.4 CG to all-atom backmapping

To calculate the hydrophobic and hydrophilic solvent accessible surface area (SASA) of the enzyme, the atoms or beads (of the surface residues) carrying a charge within the range from -0.2 to +0.2 were considered to contribute to the hydrophobic SASA and rest of the atoms or beads from the surface residues contribute to the hydrophilic SASA.[57] But, in the MARTINI force field, the charge on the nonpolar beads are set to be zero. Thus, the partitioning of the total SASA among hydrophobic and hydrophilic counterparts cannot be calculated within a CG frame work. Furthermore, in the MARTINI CG model, as the sidechain of Ala and Gly

residues are not considered as separate bead from the backbone, the hydrophobic moment (see later) calculated from a CG frame work would not be correct for these two residues. Thus, we backmapped the CG trajectories to all-atom ones by using the initram.sh script.[58] Later, the GROMACS module gmx_sasa[57] was used to calculate the total, hydrophobic and hydrophilic SASAs from the all-atom trajectories.

7.5 Validation of the MARTINI CG model

Recently, three important observations on the MARTINI model have been reported.[59] These are:

- *(i)* The absence of specific cross Lennard-Jones parameters between different particle sizes can lead to artificially high free energy barriers in the dimerization profile. In line with this observation, Javanainen et al.[60] has recently found excessive aggregation of membrane proteins in the Martini model. But, in our present study involving only one protein molecule in each system, the question of dimerization is ruled out.

- *(ii)* During parameterization of the force field for a molecule by deviating too far from the standard MARTINI bonded parameters (like using two-bead model describing octane directly for a shorter molecule like heptane; i. e., the shortening of the CG bond length) will effect the solute partitioning behaviour and solvent properties. But, all the molecule types present in our systems contain only the standard MARTINI bonded parameters. Thus this issue also does not affect our simulations.

- *(iii)* Use of too weak bonded force constants, especially while designing elastic network model for protein comes with the risk of artificially inducing clustering. But, the systems under this study contain only one protein molecule and thus this concern too is inapplicable for our study.

Thus, none of the issues related to the MARTINI CG model reported in literature affect the present study.

References

(1) Kubler, D.; Bergmann, A.; Weger, L.; Ingenbosch, K. N.; Hoffmann-Jacobsen, K. Kinetics of Detergent-Induced Activation and Inhibition of a Minimal Lipase. *J. Phys. Chem. B* **2017**, *121*, 1248–1257.

(2) Lyu, J.; Li, Z.; Men, J.; Jiang, R.; Tang, G.; Zhou, Y.; Gao, R. Covalent immobilization of Bacillus subtilis lipase A on Fe3O4 nanoparticles by aldehyde tag: An ideal immobilization with minimal chemical modification. *Process biochemistry* **2019**, *81*, 63–69.

(3) Heater, B. S.; Lee, M. M.; Chan, M. K. Direct production of a genetically-encoded immobilized biodiesel catalyst. *Scientific reports* **2018**, *8*, 12783.

(4) Verma, M. L.; Rao, N. M.; Tsuzuki, T.; Barrow, C. J.; Puri, M. Suitability of Recombinant Lipase Immobilised on Functionalised Magnetic Nanoparticles for Fish Oil Hydrolysis. *Catalysts* **2019**, *9*, 420.

(5) de Mello, M. D.; Cordeiro, D.; Costa, L. T.; Follmer, C. Catalytic properties of lipases immobilized onto ultrasound-treated chitosan supports. *Biotechnology and bioprocess engineering* **2013**, *18*, 1090–1100.

(6) Desai, P.; Dave, A.; Devi, S. Alcoholysis of salicornia oil using free and covalently bound lipase onto chitosan beads. *Food chemistry* **2006**, *95*, 193–199.

(7) Kılınç, A.; Teke, M.; Önal, S.; Telefoncu, A. Immobilization of pancreatic lipase on chitin and chitosan. *Preparative biochemistry & biotechnology* **2006**, *36*, 153–163.

(8) Tischer, W.; Wedekind, F. *Biocatalysis-from discovery to application*; Springer, 1999; pp 95–126.

(9) Paula, A. V.; Urioste, D.; Santos, J. C.; de Castro, H. F. Porcine pancreatic lipase immobilized on polysiloxane–polyvinyl alcohol hybrid matrix: catalytic properties

and feasibility to mediate synthesis of surfactants and biodiesel. *Journal of Chemical Technology & Biotechnology: International Research in Process, Environmental & Clean Technology* **2007**, *82*, 281–288.

(10) Wu, S.-C.; Wu, S.-M.; Su, F.-M. Novel process for immobilizing an enzyme on a bacterial cellulose membrane through repeated absorption. *Journal of Chemical Technology & Biotechnology* **2017**, *92*, 109–114.

(11) Arana-Peña, S.; Lokha, Y.; Fernández-Lafuente, R. Immobilization on octyl-agarose beads and some catalytic features of commercial preparations of lipase a from Candida antarctica (Novocor ADL): Comparison with immobilized lipase B from Candida antarctica. *Biotechnology progress* **2019**, *35*, e2735.

(12) Arana-Peña, S.; Lokha, Y.; Fernández-Lafuente, R. Immobilization of eversa lipase on octyl agarose beads and preliminary characterization of stability and activity features. *Catalysts* **2018**, *8*, 511.

(13) Palomo, J. M.; Muñoz, G.; Fernández-Lorente, G.; Mateo, C.; Fernández-Lafuente, R.; Guisán, J. M. Interfacial adsorption of lipases on very hydrophobic support (octadecyl–Sepabeads): immobilization, hyperactivation and stabilization of the open form of lipases. *Journal of Molecular Catalysis B: Enzymatic* **2002**, *19*, 279–286.

(14) Rios, N. S.; Arana-Peña, S.; Mendez-Sanchez, C.; Ortiz, C.; Gonçalves, L. R.; Fernandez-Lafuente, R. Reuse of Lipase from Pseudomonas fluorescens via Its Step-by-Step Coimmobilization on Glyoxyl-Octyl Agarose Beads with Least Stable Lipases. *Catalysts* **2019**, *9*, 487.

(15) Orrego, A.; Ghobadi, R.; Moreno-Perez, S.; Mendoza, A.; Fernandez-Lorente, G.; Guisan, J.; Rocha-Martin, J. Stabilization of immobilized lipases by intense intramolecular cross-linking of their surfaces by using aldehyde-dextran polymers. *International journal of molecular sciences* **2018**, *19*, 553.

(16) Kumar, A.; Zhang, S.; Wu, G.; Wu, C. C.; Chen, J.; Baskaran, R.; Liu, Z. Cellulose binding domain assisted immobilization of lipase (GSlip–CBD) onto cellulosic nanogel: characterization and application in organic medium. *Colloids and Surfaces B: Biointerfaces* **2015**, *136*, 1042–1050.

(17) Cao, S.-L.; Huang, Y.-M.; Li, X.-H.; Xu, P.; Wu, H.; Li, N.; Lou, W.-Y.; Zong, M.-H. Preparation and characterization of immobilized lipase from Pseudomonas cepacia onto magnetic cellulose nanocrystals. *Scientific reports* **2016**, *6*, 20420.

(18) Lee, D.-G.; Ponvel, K. M.; Kim, M.; Hwang, S.; Ahn, I.-S.; Lee, C.-H. Immobilization of lipase on hydrophobic nano-sized magnetite particles. *Journal of Molecular Catalysis B: Enzymatic* **2009**, *57*, 62–66.

(19) Jiang, Y.; Guo, C.; Xia, H.; Mahmood, I.; Liu, C.; Liu, H. Magnetic nanoparticles supported ionic liquids for lipase immobilization: Enzyme activity in catalyzing esterification. *Journal of Molecular Catalysis B: Enzymatic* **2009**, *58*, 103–109.

(20) Su, F.; Li, G.; Fan, Y.; Yan, Y. Enhanced performance of lipase via microcapsulation and its application in biodiesel preparation. *Scientific reports* **2016**, *6*, 29670.

(21) Weltz, J. S.; Kienle, D. F.; Schwartz, D. K.; Kaar, J. L. Dramatic Increase in Catalytic Performance of Immobilized Lipases by Their Stabilization on Polymer Brush Supports. *ACS Catalysis* **2019**, *9*, 4992–5001.

(22) Das, S.; Balasubramanian, S. pH-Induced Rotation of Lidless Lipase LipA from Bacillus subtilis at Lipase–Detergent Interface. *The Journal of Physical Chemistry B* **2018**, *122*, 4802–4812.

(23) Zeppieri, S.; Rodríguez, J.; López de Ramos, A. Interfacial tension of alkane+ water systems. *Journal of Chemical & Engineering Data* **2001**, *46*, 1086–1088.

(24) Michalowsky, J.; Schäfer, L. V.; Holm, C.; Smiatek, J. A refined polarizable water model for the coarse-grained MARTINI force field with long-range electrostatic interactions. *The Journal of chemical physics* **2017**, *146*, 054501.

(25) Yesylevskyy, S. O.; Schäfer, L. V.; Sengupta, D.; Marrink, S. J. Polarizable water model for the coarse-grained MARTINI force field. *PLoS computational biology* **2010**, *6*, e1000810.

(26) Chothia, C. The nature of the accessible and buried surfaces in proteins. *Journal of molecular biology* **1976**, *105*, 1–12.

(27) Wolfenden, R.; Andersson, L.; Cullis, P.; Southgate, C. Affinities of amino acid side chains for solvent water. *Biochemistry* **1981**, *20*, 849–855.

(28) Radzicka, A.; Wolfenden, R. Comparing the polarities of the amino acids: side-chain distribution coefficients between the vapor phase, cyclohexane, 1-octanol, and neutral aqueous solution. *Biochemistry* **1988**, *27*, 1664–1670.

(29) Eisenberg, D.; Weiss, R. M.; Terwilliger, T. C.; Wilcox, W. Hydrophobic moments and protein structure. Faraday Symposia of the Chemical Society. 1982; pp 109–120.

(30) Van Pouderoyen, G.; Eggert, T.; Jaeger, K.-E.; Dijkstra, B. W. The crystal structure of Bacillus subtili lipase: a minimal α/β hydrolase fold enzyme. *J. Mol. Biol.* **2001**, *309*, 215–226.

(31) Berman, H. M.; Westbrook, J.; Feng, Z.; Gilliland, G.; Bhat, T. N.; Weissig, H.; Shindyalov, I. N.; Bourne, P. E. *International Tables for Crystallography Volume F: Crystallography of Biological Macromolecules*; Springer, 2006; pp 675–684.

(32) DeLano, W. L. The PyMOL molecular graphics system. **2002**,

(33) Martinez-Rosell, G.; Giorgino, T.; De Fabritiis, G. PlayMolecule ProteinPrepare: A

web application for protein preparation for molecular dynamics simulations. *J. Chem. Inf. Model.* **2017**,

(34) Martínez, L.; Andrade, R.; Birgin, E. G.; Martínez, J. M. Packmol: A package for building initial configurations for molecular dynamics simulations. *J. Comput. Chem.* **2009**, *30*, 2157–2164.

(35) Periole, X.; Cavalli, M.; Marrink, S.-J.; Ceruso, M. A. Combining an elastic network with a coarse-grained molecular force field: structure, dynamics, and intermolecular recognition. *Journal of Chemical Theory and Computation* **2009**, *5*, 2531–2543.

(36) de Jong, D. H.; Singh, G.; Bennett, W. D.; Arnarez, C.; Wassenaar, T. A.; Schafer, L. V.; Periole, X.; Tieleman, D. P.; Marrink, S. J. Improved parameters for the martini coarse-grained protein force field. *Journal of Chemical Theory and Computation* **2012**, *9*, 687–697.

(37) Velinova, M.; Sengupta, D.; Tadjer, A. V.; Marrink, S.-J. Sphere-to-rod transitions of nonionic surfactant micelles in aqueous solution modeled by molecular dynamics simulations. *Langmuir* **2011**, *27*, 14071–14077.

(38) Lee, H.; de Vries, A. H.; Marrink, S.-J.; Pastor, R. W. A coarse-grained model for polyethylene oxide and polyethylene glycol: conformation and hydrodynamics. *The journal of physical chemistry B* **2009**, *113*, 13186–13194.

(39) Lee, H.; Larson, R. G. Molecular dynamics study of the structure and interparticle interactions of polyethylene glycol-conjugated PAMAM dendrimers. *The Journal of Physical Chemistry B* **2009**, *113*, 13202–13207.

(40) Euston, S. R. Molecular dynamics simulation of protein adsorption at fluid interfaces: a comparison of all-atom and coarse-grained models. *Biomacromolecules* **2010**, *11*, 2781–2787.

(41) Marrink, S. J.; Risselada, H. J.; Yefimov, S.; Tieleman, D. P.; De Vries, A. H. The MARTINI force field: coarse grained model for biomolecular simulations. *The journal of physical chemistry B* **2007**, *111*, 7812–7824.

(42) Bussi, G.; Donadio, D.; Parrinello, M. Canonical sampling through velocity rescaling. *J. Chem. Phys.* **2007**, *126*, 014101.

(43) Berendsen, H. J.; Postma, J. v.; van Gunsteren, W. F.; DiNola, A.; Haak, J. R. Molecular dynamics with coupling to an external bath. *The Journal of chemical physics* **1984**, *81*, 3684–3690.

(44) Parrinello, M.; Rahman, A. Polymorphic transitions in single crystals: A new molecular dynamics method. *J. Appl. Phys.* **1981**, *52*, 7182–7190.

(45) Nosé, S.; Klein, M. L. Constant pressure molecular dynamics for molecular systems. *Mol. Phys.* **1983**, *50*, 1055–1076.

(46) Darden, T.; York, D.; Pedersen, L. Particle mesh Ewald: An Nlog(N) method for Ewald sums in large systems. *J. Chem. Phys.* **1993**, *98*, 10089–10092.

(47) Bekker, H.; Berendsen, H.; Dijkstra, E.; Achterop, S.; Van Drunen, R.; Van der Spoel, D.; Sijbers, A.; Keegstra, H.; Reitsma, B.; Renardus, M. Gromacs: A parallel computer for molecular dynamics simulations. Physics computing. 1993; pp 252–256.

(48) Berendsen, H. J.; van der Spoel, D.; van Drunen, R. GROMACS: a message-passing parallel molecular dynamics implementation. *Comput. Phys. Commun.* **1995**, *91*, 43–56.

(49) Lindahl, E.; Hess, B.; Van Der Spoel, D. GROMACS 3.0: a package for molecular simulation and trajectory analysis. *J. Mol. Model.* **2001**, *7*, 306–317.

(50) Van Der Spoel, D.; Lindahl, E.; Hess, B.; Groenhof, G.; Mark, A. E.; Berendsen, H. J. GROMACS: fast, flexible, and free. *J. Comput. Chem.* **2005**, *26*, 1701–1718.

(51) Hess, B.; Kutzner, C.; Van Der Spoel, D.; Lindahl, E. GROMACS 4: algorithms for highly efficient, load-balanced, and scalable molecular simulation. *J. Chem. Theory Comput.* **2008**, *4*, 435–447.

(52) Pronk, S.; Páll, S.; Schulz, R.; Larsson, P.; Bjelkmar, P.; Apostolov, R.; Shirts, M. R.; Smith, J. C.; Kasson, P. M.; van der Spoel, D. GROMACS 4.5: a high-throughput and highly parallel open source molecular simulation toolkit. *Bioinformatics* **2013**, *29*, 845–854.

(53) Torrie, G. M.; Valleau, J. P. Nonphysical sampling distributions in Monte Carlo free-energy estimation: Umbrella sampling. *Journal of Computational Physics* **1977**, *23*, 187–199.

(54) Hub, J. S.; De Groot, B. L.; Van Der Spoel, D. g_wham A Free Weighted Histogram Analysis Implementation Including Robust Error and Autocorrelation Estimates. *Journal of chemical theory and computation* **2010**, *6*, 3713–3720.

(55) Jarzynski, C. Nonequilibrium equality for free energy differences. *Physical Review Letters* **1997**, *78*, 2690.

(56) Park, S.; Schulten, K. Calculating potentials of mean force from steered molecular dynamics simulations. *The Journal of chemical physics* **2004**, *120*, 5946–5961.

(57) Eisenhaber, F.; Lijnzaad, P.; Argos, P.; Sander, C.; Scharf, M. The double cubic lattice method: efficient approaches to numerical integration of surface area and volume and to dot surface contouring of molecular assemblies. *Journal of Computational Chemistry* **1995**, *16*, 273–284.

(58) Wassenaar, T. A.; Pluhackova, K.; Bockmann, R. A.; Marrink, S. J.; Tieleman, D. P. Going backward: a flexible geometric approach to reverse transformation from coarse grained to atomistic models. *Journal of chemical theory and computation* **2014**, *10*, 676–690.

(59) Alessandri, R.; Souza, P. C. T.; Thallmair, S.; Melo, M. N.; de Vries, A. H.; Marrink, S. J. Pitfalls of the Martini Model. *Journal of Chemical Theory and Computation* **2019**, *15*, 5448–5460.

(60) Javanainen, M.; Martinez-Seara, H.; Vattulainen, I. Excessive aggregation of membrane proteins in the Martini model. *PLoS One* **2017**, *12*, e0187936.